The Journal of Chemical Physics

RESEARCH ARTICLE | JANUARY 31 2024

A hybrid quantum–classical theory for predicting terahertz charge-transfer plasmons in metal nanoparticles on graphene

A. S. Fedorov ; E. V. Eremkin ; P. O. Krasnov ; V. S. Gerasimov ; H. Ågren ; S. P. Polyutov

J. Chem. Phys. 160, 044117 (2024)
https://doi.org/10.1063/5.0178247

The Journal of Chemical Physics ARTICLE pubs.aip.org/aip/jcp

A hybrid quantum–classical theory for predicting terahertz charge-transfer plasmons in metal nanoparticles on graphene

Cite as: J. Chem. Phys. 160, 044117 (2024); doi: 10.1063/5.0178247
Submitted: 26 September 2023 • Accepted: 7 January 2024 •
Published Online: 31 January 2024

A. S. Fedorov,[1,2,a] E. V. Eremkin,[1] P. O. Krasnov,[1] V. S. Gerasimov,[3] H. Ågren,[4] and S. P. Polyutov[1,b]

AFFILIATIONS

[1] International Research Center of Spectroscopy and Quantum Chemistry, Siberian Federal University, 660041 Krasnoyarsk, Russia
[2] Kirensky Institute of Physics, Federal Research Center KSC SB RAS, 660036 Krasnoyarsk, Russia
[3] Institute of Computational Modeling SB RAS, 660036 Krasnoyarsk, Russia
[4] Department of Physics and Astronomy, Uppsala University, Box 516, SE-751 20 Uppsala, Sweden

[a] **E-mail:** qchem99@yandex.ru
[b] **Author to whom correspondence should be addressed:** spolyutov@sfu-kras.ru

ABSTRACT

Metal nanoparticle (NP) complexes lying on a single-layer graphene surface are studied with a developed original hybrid quantum–classical theory using the Finite Element Method (FEM) that is computationally cheap. Our theory is based on the motivated assumption that the carrier charge density in the doped graphene does not vary significantly during the plasmon oscillations. Charge transfer plasmon (CTP) frequencies, eigenvectors, quality factors, energy loss in the NPs and in graphene, and the absorption power are aspects that are theoretically studied and numerically calculated. It is shown the CTP frequencies reside in the terahertz range and can be represented as a product of two factors: the Fermi level of graphene and the geometry of the NP complex. The energy losses in the NPs are predicted to be inversely dependent on the radius R of the nanoparticle, while the loss in graphene is proportional to R and the interparticle distance. The CTP quality factors are predicted to be in the range ~10 – 100. The absorption power under CTP excitation is proportional to the scalar product of the CTP dipole moment and the external electromagnetic field. The developed theory makes it possible to simulate different properties of CTPs 3–4 orders of magnitude faster compared to the original FEM or the finite-difference time domain method, providing possibilities for predicting the plasmonic properties of very large systems for different applications.

INTRODUCTION

Recent innovations in nanotechnology and photonics show that Terahertz (THz) radiation (300 GHz to 30 THz frequencies, or 1 mm–30 μm wavelength) can be considered in many applications.[1] The THz research relies on the unique ability of this radiation to penetrate through different materials with little attenuation, such as paper, plastic, clothes, wood, and ceramics, which are usually opaque at optical wavelengths. THz radiation can be used to accurately detect many molecules of interest based on distinctive rotational/vibrational resonances in its frequency region.[2] Thus, THz technology has become of use in a wide variety of applications, such as for detection of drugs and explosives, for security screening, in spectroscopy and imaging communication technology, in biology and medical sciences,[3] for quality control of different agricultural products, and for global environmental monitoring.[4] THz imaging devices can be used for nondestructive testing for hidden object detection, which is harmless for humans in contrast to x rays.

Despite significant recent progress, the key challenge limiting the widespread adoption of these technologies remains in the development of practical THz optoelectronic devices, especially radiation

sources. It is well known that, while the THz spectral region lies at the boundary between the traditional domains of photonics and microwave electronics, device concepts borrowed from either discipline cannot be readily extended to THz frequencies. In particular, microwave sources are generally restricted to operation frequencies below ~1 THz because of the small size of elements, which is typical for magnetrons or because of the limitations of the main materials for traditional semiconductors, such as low mobility and saturation velocity.[5] On the other hand, THz quantum cascade lasers (QCLs) established using gallium arsenide quantum wells show a relatively good performance.[6] However, their spectral range is restricted to a limited portion of the THz spectrum (currently 1.2–5.4 THz) due to strong GaAs lattice absorption at frequencies outside this band.

Additionally, their operating temperatures are fundamentally limited to ~200 K, so cooling is required for high-performance operation, which strongly restricts their portability and integration into practical systems.[7] So, at present, the most practical THz spectroscopy and imaging systems are based on photoconductive antennas for THz wave generation.[8] However, the operation of these devices requires an ultrafast laser source (usually fiber based or Ti:sapphire), which leads to essential increases in their size, power consumption, complexity, and cost.

For the past several years, significant research efforts have reported graphene as a very promising material for THz optoelectronics and other applications. In Ref. 9, it was pointed out that graphene plasmons provide a suitable alternative to noble-metal plasmons. This is a consequence of the fact that these plasmons exhibit a much tighter confinement and long propagation distances in comparison with noble-metal plasmons. This makes it possible to use graphene as a platform for strongly enhanced light–matter interactions and to construct single-molecule plasmon devices. Graphene began to be considered as such a plasmon material due to its unique properties—a gapless and linear energy dispersion near the Dirac points. This feature covers the entire THz and infrared regions.[10–12] Theoretical and experimental studies have shown that relaxation dynamics of hot carriers in graphene exhibits an unusual twofold nature: They rapidly ($\tau \leq 100$ fs) thermalize the longitudinal distribution relative to the Dirac point, while a noncollinear scattering is much slower ($\tau \sim$ ps) when low energy optical phonons are excited.[13,14] The long scattering time is very promising for infrared and THz devices based on hot carrier effects, which implies that graphene possesses ballistic electronic transport over μm-scale distances with a record large room-temperature mobility,[14–16] making graphene a very perspective material for THz sources based on coherent carrier dynamics.[17] It has been predicted that the graphene conductivity μ can reach a value as high as 200 000 cm^2/Vs, which is the highest value reported in the literature.[14] This μ value was obtained at electron densities of $n = 2 \times 10^{11}$ cm^{-2} in a single layer graphene sample suspended at 150 nm above a Si/SiO_2 gate electrode. At the same time, for unsuspended devices, a mobility of 25 000 cm^2/Vs has been reached, which is close to the highest carrier mobility $\mu > 10^4$ cm^2/Vs at room temperature mentioned in the literature.[18]

A very important and interesting graphene feature, discussed in this work, is the existence of graphene plasmonic resonances at THz or mid-infrared frequencies, something that is very different from the traditional plasmonic nanostructures based on noble metals having plasmons in the visible or near-infrared excitations.[11,19,20] Graphene plasmon polaritons (GPPs), having a strong field confinement and large propagation lengths, are effectively tunable using gate voltage to control the free carrier density, which is particularly attractive for optoelectronic device applications.[21]

Using the fact that in the THz or mid-infrared frequency range, the intraband contribution to the optical conductivity $\sigma_{intra}(\omega, E_f)$ of graphene is much higher than the interband one, i.e., using the Drude approximation,[22] it has been shown that the graphene plasmon frequency depends on the square root ($\omega \sim \sqrt{q}$) of the plasmon wave vector q. For the discussed frequency range, this means that the graphene plasmon wave vector q is about two orders of magnitude larger than q_0 of free space photons. It leads to a significant confinement of variable electrical and magnetic fields in the graphene. At the same time, although it is difficult to obtain an effective energy transfer from electromagnetic field (EMF) to graphene, regular gratings of metal nanoparticles (NPs) on graphene surfaces have been used for this purpose. However, available information about such systems describes situations where the size of the NPs and the array period matches $\lambda \sim \mu$m,[23] which makes it possible to excite plasmons in graphene with the corresponding wavelength and frequencies of a few terahertz.

In this work, we consider systems of metal NPs of nanometer size, lying on the single layer graphene, as shown in Fig. 3. We show that in these systems, charge transfer plasmons (CTPs) can be excited when charges periodically oscillate between the NPs, causing a periodic change of a potential energy of charged NPs and periodic change of a kinetic energy of charges moving in the graphene.

DFTB/NEGF INVESTIGATION OF SYSTEMS CONSISTING OF METAL NANOPARTICLES LYING ON GRAPHENE

It is necessary to certify that there is sufficient conductivity between the nanoparticle and the graphene. For this purpose, a precise simulation of the graphene–NP contact transmission was carried out using the non-equilibrium Green's function (NEGF) method,[24] which is available in the DFTB+ software package.[25] All calculations were carried out using the SCC-DFTB method[26] and the *auorg* set of parameters[26,27] for the description of interatomic interactions. Since the magnetic properties of the system are beyond the scope of our study, spin polarization was not considered in our calculations. Geometry optimization, when performed, was carried out for an energy gradient threshold of 1×10^{-4} a.u., taking into account the dispersion interaction by using the DFT-D3 approach.[28,29]

The considered "electrode–NP–graphene–NP–electrode" system was generated consisting of two semi-infinite gold electrodes (blue atoms) connected to gold nanoparticles (red atoms) in contact with the graphene, as shown in Fig. 1. The procedure of this system creation included a few steps.

In the first step, we simulated graphene considering a unit cell containing two atoms. Its geometry was optimized, and as a result, the following parameters were obtained: $a = b = 2.47$ Å, $\gamma = 120°$, which only slightly differ from the well-known values ($a = b = 2.46$ Å). Since the cell was located in the xy plane, and the calculations from a technical point of view assume periodicity in 3D space, a constant vacuum gap of 60 Å long was set along the z axis

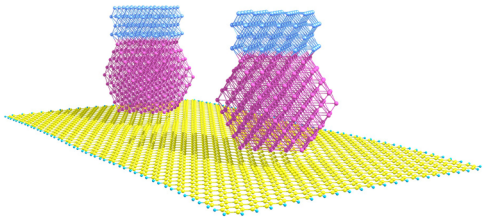

FIG. 1. Geometry of the "electrode–NP–graphene–NP–electrode" system.

in order to avoid the interaction of atoms with their images from neighboring cells along the direction perpendicular to the surface. In fact, this means that c = 60 Å and $\alpha = \beta = 90^\circ$. Next, a rectangular graphene supercell, containing 1032 atoms, was created by translating along the x and y directions of the graphene unit cell. The supercell had the following parameters: a = 51.34 Å, b = 51.87 Å, and angle $\gamma = 90^\circ$.

In the second step, a preliminary optimized cuboctahedral gold nanoparticle consisting of 309 atoms, oriented with a square face toward the graphene surface, was placed above the center of the graphene fragment. After that, the positions of all carbon and gold atoms were relaxed, taking into account the periodic conditions. Since a vacuum gap of 60 Å was specified along the z direction, c = 60 Å and $\alpha = \beta = 90^\circ$. The key aim of this step was to optimize the position of the atoms at the site of contact between the nanoparticle and the graphene.

In the third step, a gold electrode in the form of four gold layers was added to the top of the gold nanoparticle. It was extracted from the corresponding crystal with known crystal parameters ($a = b = c$ = 4.0782 Å; $\alpha = \beta = \gamma = 90^\circ$). In further calculations of the transmission coefficient, this electrode was considered semi-periodic, i.e., it was, in fact, a cylinder, whose diameter was approximately equal to the diameter of the nanoparticle, and had a periodicity upward from the nanoparticle along the z direction. In this case, it was placed in such a way that the distance from the bottom face to the top face of the nanoparticle was equal to the distance between the corresponding gold layers in the crystal.

In the fourth and final step, the entire resulting "graphene–NP–electrode" system was translated once along the x axis to ultimately construct a model of a device containing graphene connected to nanoparticles with attached electrodes—"electrode–NP–graphene–NP–electrode." Since this model was considered a cluster without periodic conditions, the broken chemical bonds along the edges of the graphene fragment were closed by hydrogen atoms, whose positions also were optimized. As a result, the entire system, not counting electrodes, consisted of 2064 carbon atoms, 618 gold atoms, and 138 hydrogen atoms. NPs were connected with the graphene surface by a square facet so that one of its diagonals was parallel to the line connecting the center projections of the NPs. The length of the facet diagonal was equal 15.59 Å, so we can assume that the area of the NP–graphene contact spot is equal to 121.5 Å^2.

After constructing the "electrode–NP–graphene–NP–electrode" geometry, the energy dependence of transmittance $T(E)$ through the system was calculated using the NEGF method (see Fig. 2). For that, the energy range $(E_{fermi} - 0.6\ \text{eV} \ldots E_{fermi} + 0.6\ \text{eV})$

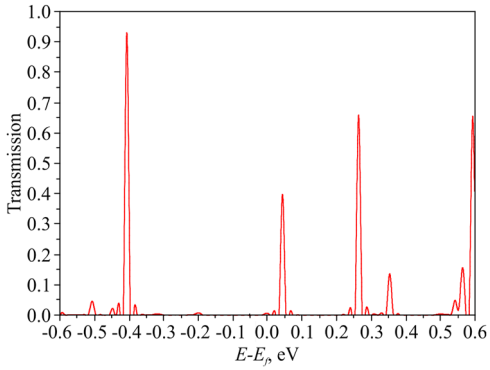

FIG. 2. Conductivity $T(E)$ of the "electrode–NP–graphene–NP–electrode" system.

was divided into intervals of 0.001 eV. This interval is ~20 times smaller than k_bT at room temperature, which guarantees a correct calculation of the integral and the system conductivity G at this temperature [see Eq. (1) below].

To find the total conductivity of the NP–graphene interface G_i, we assume that this conductivity is determined by twice the total conductivity of the "electrode–NP–graphene–NP–electrode" system G. To calculate it, the following formula based on the Landauer formalism[30] within the linear approximation was used:

$$G = \frac{I}{\phi_2 - \phi_1} = \frac{2e^2}{h} \int_{-\infty}^{\infty} T(E) \frac{\partial f_0(E,T)}{\partial E} dE, \qquad (1)$$

where the Fermi function reads $f_0(E,T) = \left[\frac{1}{\exp((E-\mu)/k_bT)+1}\right]_{\mu=E_{fermi}}$.

Using the above equation, the total NP–graphene interface conductivity $G_i \simeq 0.48\frac{2e^2}{h}$ in conductivity quantum values was found, which means that the conductivity is sufficiently good even for such a small NP–graphene contact spot. Therefore, we can assume that with an increase in the NP size and the corresponding contact spot increase, the G_i value will be increased proportionally. That is why in further calculations, we do not consider the resistance of the NP–graphene interface but only take into account the conductivity of the graphene.

THEORY OF CHARGE TRANSFER PLASMONS IN NP-GRAPHENE COMPLEXES

In this work, we further develop the hybrid quantum–classical model first used in Refs. 31 and 32. This model described CTPs in systems with metal nanoparticles connected by bridges (linkers) consisting of a narrow conductive molecular polymer chain and where the conductive carriers move in a ballistic mode. The harmonically changing current of the ballistically moving carriers accumulate kinetic energy, which is periodically pumped into the potential energy of charged nanoparticles. The kinetic energy of the bridge E_{kin} can be written as a sum over electrons in the conduction band: $E_{kin} = \sum_{k,n} n_{k,n} \frac{\hbar^2 k_{k,n}^2}{2m^*}$, where $n_{k,n}$ denotes the occupation degrees of electrons having quasi-momentum k_k and band number n and m^* is the carrier effective mass. Here, a parabolic dependence

of the electron's kinetic energy from k_k is assumed. Under the influence of a weak electric field, the carriers are excited only near the Fermi level, so the kinetic energy derivative reads as follows: $\frac{dE_{kin}}{dt} = n_f \frac{\hbar k}{m^*}\left[\frac{d(\hbar k)}{dt}\right]_{k=k_f}$. In the present work, we extend this model for systems where metal NPs lie on a graphene sheet, i.e., they are connected by an infinitely extended and conductive medium. Similar to the previous model, the free carriers move in the graphene mainly ballistically, while maintaining the original charge density during the CTP excitations. The presence of a conductive surface leads to the appearance of a continuum of paths for charge movement between the NPs, which fundamentally distinguishes this model from the previous model.

In view of the consideration of the terahertz frequency range, which is much smaller than the optical range, it is natural to use the quasi-stationary approximation. In this approximation, the Maxwell bias current is much smaller than the conduction current $|\frac{\partial D}{\partial t}| \ll |j(r)|$, so the charges in the graphene and in the volume of nanoparticles can be neglected. In addition, unlike in the previous model, the free carriers in a single-layer graphene are massless fermions near the Dirac cones.[33,34]

As the basis of a model being developed for describing plasmons, like the previous model, we assume the conservation of the total energy $E_{tot} = E_{pot} + E_{kin}$ of an NP–graphene system. So, the main equation is as follows:

$$\frac{dE_{tot}}{dt} = \frac{dE_{pot}}{dt} + \frac{dE_{kin}}{dt} = 0. \tag{2}$$

The total energy consists of the electrostatic energy of interaction between charged nanoparticles $E_{pot} = E_{NP}$ and the kinetic energy of the nonequilibrium charges in graphene. Here, we assume that the equilibrium charge density in graphene $\rho_{equil}(r)$, arising due to its doping or gating, does not change and that it is much higher than the nonequilibrium density $\rho_{nonequil}(r)$ under the plasmon excitations,

$$\rho_{equil}(r) = const \gg \rho_{nonequil}(r).$$

To prove this contention, one can consider the continuity equation, which can be written for harmonic oscillations as $\vec{\nabla}\vec{j}(r) = -e\frac{\partial \rho(r)}{\partial t} = -ie\omega\rho(r)$, where $\vec{j}(r)$ is the current density in graphene, $\rho(r)$ is the charge density there, and ω is the CTP oscillation frequency. Because the density is the sum of the static equilibrium, and changing nonequilibrium densities $\rho(r) = \rho_{equil} + \rho_{nonequil}(r)$ and presenting $\vec{j}$ as the product of $\rho(r)$ and a carriers group velocity V_{group}, one can rewrite this equation as $\vec{\nabla}\left(\rho_{equil} + \rho_{nonequil}(r)\right)\vec{V}_{group}(r)\big) = -i\omega(\rho_{nonequil}(r)$. Because of a low density of states (DOS) of graphene near the Dirac points, the carrier's effective group velocity V_{eff} is much smaller than $V_{fermi} \simeq 10^6$ m/s,[35] where $V_{eff} \simeq 1.4 \times 10^5$ m/s has been measured. Using estimation $\vec{\nabla} \sim \frac{1}{L}$, where L is the system size, one can obtain $(\rho_{equil} + \rho_{nonequil}(r)) \sim \frac{\omega L}{V_{eff}}\rho_{nonequil}$. For a characteristic plasmon frequency of $\nu = 15$ THz and $L = 100$ nm, one can estimate $\rho_{nonequil}(r) \sim 0.014\rho_{equil}$, which proves the assumption that the charge density in graphene is not changed because of the CTPs.

Thus, we assume that the graphene possesses only the kinetic energy of the nonequilibrium carriers, while its potential energy can be omitted: $E_{Graphene} = E_{Kin}$. As in the section describing CTPs in systems of metal nanoparticles joined by conductive linkers, we assume that there are metal nanoparticles at the points with coordinates R_i, of which the charge during the plasmon oscillations changes according to the following harmonic law $Q_i(t) = Q_i e^{i\omega t}$, where Q_i is the amplitude of charge in a point having coordinates R_i. Although all charges have the same oscillating factor $e^{i\omega t}$, their amplitudes Q_i may be different. Due to the fact that the nanoparticles lie on the graphene surface, this charge flows over the graphene surface between the nanoparticles while storing the kinetic energy, which also changes according to the harmonic law. Here and in the following, we assume that the radius of all particles is R and that each particle has a contact spot of radius R_0 with graphene, outside of which the current flowing from the nanoparticle spreads over the graphene surface, as shown in Fig. 3.

Under these assumptions, the potential energy time derivative is as follows:

$$\begin{aligned}\frac{dE_{pot}}{dt} &= \frac{d}{dt}\left[\sum_i \frac{Q_i^2}{2R} + \sum_{i<j}\frac{Q_iQ_j}{|R_i - R_j|}\right] \\ &= 2i\omega\left[\sum_i \frac{Q_i^2}{2R} + \sum_{i<j}\frac{Q_iQ_j}{|R_i - R_j|}\right] = i\omega\sum_{i,j} A_{i,j}Q_iQ_j, \\ A_{i,j} &= \frac{\delta_{i,j}}{R} + \frac{2}{|R_i - R_j|_{i\neq j}}.\end{aligned} \tag{3}$$

The time derivative of the density kinetic energy of induced carriers in graphene is determined by the external work A of electrostatic forces on these carriers,[36] taken with the opposite sign,

$$\frac{dE_{kin}}{dVdt} = -\frac{1}{2}j(r,\omega)E_{\parallel}^*(r,\omega) = -\frac{1}{2}\sigma(\omega,\mu,T)|E_{\parallel}(r,\omega)|^2. \tag{4}$$

Here, $\sigma(\omega, \mu, T)$ is the conductivity of graphene, dependent on frequency ω, chemical potential μ, and temperature T. This value can be derived from the Kubo formula[37] expressing the conductivity as the sum of intraband and interband contributions: $\sigma(\omega, \mu, T) = \sigma_{intra} + \sigma_{inter}$. For gated or highly doped graphene ($\mu \gg kT$), the chemical potential can be expressed as $\mu \simeq E_f$. In this case, the intraband graphene conductivity has the Drude-like form,[38]

$$\sigma_{intra}(\omega, E_f) = \frac{e^2E_f}{\pi\hbar^2}\frac{i}{\omega + i\tau^{-1}}, \tag{5}$$

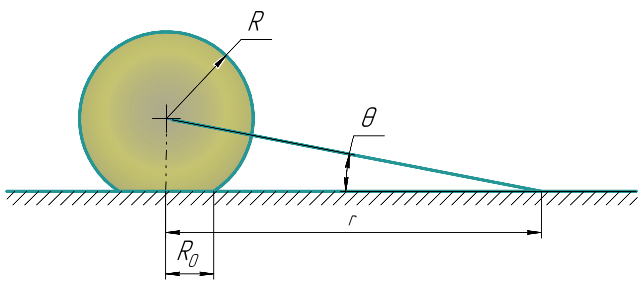

FIG. 3. NP on the graphene; r is defined as the projection of NP center onto the graphene plane, R is the NP radius, θ is the angle between r and the radius of the vector coming out of the NP's center.

where τ is the relaxation time of the free carriers momentum.

Similarly, the σ interband contribution is[37,39]

$$\sigma_{inter}(\omega, E_f) = \frac{e^2}{4\hbar}\left[\Theta(\hbar\omega - 2E_f) + \frac{i}{\pi}\ln\left|\frac{\hbar\omega - 2E_f}{\hbar\omega + 2E_f}\right|\right], \quad (6)$$

where $\Theta(\cdots)$ is the step function and the graphene Fermi level is

$$E_f = \hbar V_f \sqrt{\pi\rho}, \quad (7)$$

and the Fermi level speed is $V_f = 10^8$ cm/s. Following the equations above and the graphene optical absorption experiment,[40] it is easy to find that the intraband graphene conductivity σ_{intra} dominates in the far-infrared (FIR) and THz regions, while in the visible (VIS) and near-infrared (NIR) regions, it is dominated by the interband σ_{inter} conductivity. By this reason, in solving Eq. (4), we replaced the graphene total conductivity with its intraband conductivity (5).

Hereafter, the quantities denoted by the indices $\parallel$ and $\perp$ represent the longitudinal and normal projections with respect to the graphene plane, respectively. To determine the total derivative of the kinetic energy, it is necessary to integrate (8) over the area occupied by graphene Ω, which we take to be infinite,

$$\frac{dE_{kin}}{dt} = -\frac{1}{2}\sigma_{intra}(\omega, E_f)\int_\Omega |E_\parallel(r,\omega)|^2 d^2r = -\frac{1}{2}\sigma_{intra}(\omega, E_f)\int_\Omega \vec{\nabla}_\parallel \cdot (\varphi(r)\vec{\nabla}_\parallel\varphi(r))\, d^2r. \quad (8)$$

It should be noted that the region Ω does not include circles of radius R_0 (see Fig. 3 and its caption). For 2D integral calculations, it is natural to use the 2D divergence theorem, which is a generalization of the 3D Gauss–Ostrogradsky theorem for the case of 2D space.[41] The 2D divergence theorem states that the flux of $\vec{F}$ through the boundary curve C is the same as the double integral of div$(\vec{F})$ over the full region R,

$$\int_C \vec{F}\vec{n}\, ds = \iint_R \vec{\nabla}\cdot\vec{F}\, d^2r. \quad (9)$$

For 2D integral calculation in (8), one can use the following identity:

$$\iint_\Omega (\vec{\nabla}_\parallel\varphi(r))\cdot(\vec{\nabla}_\parallel\varphi(r))d^2r \equiv \iint_\Omega \vec{\nabla}_\parallel\cdot(\varphi(r)\vec{\nabla}_\parallel\varphi(r))d^2r - \iint_\Omega \varphi(r)(\vec{\nabla}_\parallel^2\varphi(r))d^2r. \quad (10)$$

To calculate the second term on the right-hand side of Eq. (10), one can use the Poisson equation, $\vec{\nabla}^2\varphi(r) = \vec{\nabla}_\parallel^2\varphi(r) + \vec{\nabla}_\perp^2\varphi(r) = -4\pi\rho(r)$. So, the second term of (10) is proportional to $const\cdot\int_\Omega \varphi(r)d^2r$ and must be equal to zero due to the electroneutrality of the system. The second argument here is that when calculating this contribution, the second derivatives of the potential $\vec{\nabla}_\parallel^2\varphi(r) = (\frac{d^2}{dx^2} + \frac{d^2}{dy^2})\varphi(r)$ in the graphene plane are much smaller than the contribution $\vec{\nabla}_\perp^2\varphi(r) = \frac{d^2}{dz^2}\varphi(r)$ due to the fact that the graphene thickness is much smaller than the scale of the lateral changes of the potential; therefore, the last term in (10) is $\left|\int_\Omega \varphi(r)\vec{\nabla}_\parallel^2\varphi(r)d^2r\right| \ll \left|\int_\Omega \varphi(r)(\vec{\nabla}_\parallel^2 + \vec{\nabla}_\perp^2)\varphi(r)d^2r\right| = 4\pi\int_\Omega \varphi(r)\rho(r))d^2r \equiv E_{pot}$ and can be omitted. To calculate the first term on the right-hand side of (10), we use the following equation:

$$\iint_\Omega (\vec{\nabla}_\parallel\varphi(r))\cdot(\vec{\nabla}_\parallel\varphi(r))d^2r \equiv \iint_\Omega \vec{\nabla}_\parallel\cdot(\varphi(r)\vec{\nabla}_\parallel\varphi(r))d^2r = \int_C \varphi(r)\vec{\nabla}_\parallel\varphi(r)ds, \quad (11)$$

where the contour border C consists of circles of radius R_0 around the center of contact NP–graphene. Remembering that the potential is created by charged nanoparticles with coordinates $Q_i(R_i)$ and taking into account that the electric field $E_{\rho\parallel}(r) = -\vec{\nabla}_\parallel\varphi(r)$, Eq. (11) is transformed as

$$\int_C \varphi(r)\vec{\nabla}_\parallel\varphi(r)ds = -\sum_k \int_0^{2\pi} \vec{n}(r-R_k)\varphi(r)\vec{\nabla}_\parallel(\varphi(r)d\phi = \sum_k \int_0^{2\pi}\vec{n}(r-R_k) \times \sum_{ij}\left[\frac{Q_i}{|r-R_i|}\frac{Q_j}{|r-R_j|^2}\frac{\vec{r}-\vec{R}_j}{|r-R_j|}\right]d\phi, \quad (12)$$

where any normalized vector $\vec{n}(R) = \frac{\vec{R}}{|R|}$ and integration takes place over the angle ϕ for circles of fixed radius R_0. Shifting the origin to the point R_k, Eq. (8) is transformed as

$$\frac{dE_{kin}}{dt} = -\frac{1}{2}\sigma_{intra}(\omega, E_f)\sum_k \int_0^{2\pi}\vec{n}(r)\sum_{ij}\frac{Q_iQ_j(\vec{r}-\vec{R}_{jk})}{|r-R_{ik}||r-R_{jk}|^3}d\phi, \quad (13)$$

where $\vec{R}_{jk} = \vec{R}_j - \vec{R}_k$. Due to the fact that when integrating the radius vector $\vec{r}$ changes in circles of a radius R_0 and assuming $R_0 \ll |\vec{R}_{jk}|$, one can use the Taylor series expansion: $\frac{1}{|r-R_{jk}|^3} = \frac{1}{|R_{jk}|^3}\left[1 + \frac{3\vec{r}\vec{n}_{jk}}{|R_{jk}|}\right]$, where $\vec{n_{jk}} = \frac{\vec{R_{jk}}}{|R_{jk}|}$. Using this expansion, Eq. (13) is transformed as

$$\frac{dE_{kin}}{dt} = -\sigma_{intra}(\omega, E_f)\sum_{i,j} B_{i,j}Q_iQ_j, \quad (14)$$

where the symmetrical matrix $B_{i,j}$ is defined as

$$B_{i,j} = \sum_{k\neq i\neq j}\frac{R_0}{R_{ik}R_{jk}^3}\left[-\pi + \cos(\vec{R_{ik}}, \vec{R_{jk}})\left(\frac{3\pi R_0^2}{R_{ik}R_{jk}} - \pi\frac{R_{jk}}{R_{ik}}\right)\right]_{i\rightleftarrows j} + \sum_{k=i\neq j}\frac{-\pi}{R_{jk}^3}\Bigg|_{i\rightleftarrows j}\sum_{k=j\neq i}\frac{2\pi}{R_{ik}R_0^2}\Bigg|_{i\rightleftarrows j} + \sum_{k\neq i=j}\frac{-2\pi R_0}{R_{ik}^4} + \sum_{k=i=j}\frac{2\pi}{R_0^3}. \quad (15)$$

TABLE I. CTP frequencies ν_i, dipole corrections of the frequencies $\Delta\nu_{dip}$, and normalized absorption coefficients ($W^{x,y}_{ext}$, $dP^{x,y}_{ext}$) are calculated by two methods. $W^{x,y}_{ext}$ are calculated by using Eq. (28), and $dP^{x,y}_{ext}$ are calculated by using Eq. (29).

Mode	ν, 10^{13} Hz	$\Delta\nu_{dip}$, 10^{11} Hz	x W^{x}_{ext} dP^{x}_{ext}	y W^{y}_{ext} dP^{y}_{ext}	Mode	ν, 10^{13} Hz	$\Delta\nu_{dip}$, 10^{11} Hz	x W^{x}_{ext} dP^{x}_{ext}	y W^{y}_{ext} dP^{y}_{ext}
		Dimer					Circle 12		
1	1.26	1.53	1.0000 1.0000	0.0000 0.0000	1	1.32	2.77	0.0000 0.0000	0.0000 0.0000
		Square			2	1.31	2.46	0.0000 0.0000	0.0000 0.0000
1	1.31	2.60	0.0000 0.0000	0.0000 0.0000	3	1.31	2.46	0.0000 0.0000	0.0000 0.0000
2	1.23	0.39	0.0580 0.0580	1.0000 1.0000	4	1.28	1.58	0.0000 0.0000	0.0000 0.0000
3	1.23	0.39	0.9983 0.9983	0.0000 0.0000	5	1.28	1.58	0.0000 0.0000	0.0000 0.0000
		Hexagon			6	1,22	0,21	0.0000 0.0000	0.0000 0.0000
1	1.32	2.71	0.0000 0.0000	0.0000 0.0000	7	1.22	0.21	0.0000 0.0000	0.0000 0.0000
2	1.28	1.59	0.0000 0.0000	0.0000 0.0000	8	1.15	−1.49	0.0000 0.0000	0.0000 0.0000
3	1.28	1.59	0.0000 0.0000	0.0000 0.0000	9	1.15	−1.49	0.0000 0.0000	0.0000 0.0000
4	1.15	−1.37	0.9967 0.9967	0.0000 0.0000	10	1.04	−3.23	0.0130 0.0130	1.0000 1.0000
5	1.15	−1.37	0.0815 0.0815	1.0000 1.0000	11	1.04	−3.23	0.9999 0.9999	0.0000 0.0000
		Chain 7					Grid 5 × 5		
1	1.32	2.60	0.0000 0.0109	0.0000 0.0000	1	1.35	3.91	0.0000 0.0018	0.0000 0.0019
2	1.30	2.07	0.1855 0.0981	0.0000 0.0000	2	1.34	3.32	0.0026 0.0099	0.0028 0.0103
3	1.26	1.20	0.0000 0.0347	0.0000 0.0000	3	1.34	3.32	0.0025 0.0094	0.0029 0.0107
4	1.21	0.12	0.4300 0.2672	0.0000 0.0000			...		
5	1.15	−1.25	0.0000 0.0677	0.0000 0.0000	23	0.96	−6.11	0.6766 0.6649	0.0811 0.6429
6	1.07	−2.48	0.8835 0.9555	0.0000 0.0000	24	0.96	−6.11	0.7064 0.7162	0.6755 0.6327

Here, notation $i \rightleftarrows j$ denotes the sum of two terms, where in the second term, there has been a rotation of indices i and j. Using Eqs. (2), (3), and (14), one can get the following secular equation:

$$\sum_{i,j}\left[i\omega Q_i A_{i,j} Q_j - \sigma_{intra}(\omega, E_f) Q_i B_{i,j} Q_j\right] = 0. \tag{16}$$

Neglecting the processes of carrier dissipation in Eq. (5), that is, $\tau \to \infty$, this equation can be written in matrix form as

$$\alpha\omega^2\hat{A} - \hat{B} = 0, \quad \text{where } \alpha = \frac{\pi\hbar^2}{e^2 E_f}. \tag{17}$$

Multiplying this equation by $\hat{A}^{-1}$, we arrive at the following secular equation:

$$\omega^2\hat{I} = \frac{\hat{A}^{-1}\hat{B}}{\alpha} \Longrightarrow \omega_i^2 = \frac{e^2 E_f}{\pi\hbar^2} \cdot \text{eigenvalues}(\hat{A}^{-1}\hat{B})$$
$$= \frac{e^2 V_f \sqrt{\rho}}{\sqrt{\pi}\hbar} \text{ eigenvalues } (\hat{A}^{-1}\hat{B}). \tag{18}$$

One can see that the squares of plasmon frequencies are factorized, i.e., they are represented as a product of a function depending on the density of carriers in graphene and depending on the NPs coordinate function. Based on the assumption that the contribution of dipole–monopole and dipole–dipole interactions is small, we use the approach proposed in our previous work,[42] which takes into account the dipole contributions in the CTP frequencies. These contributions are represented as

$$\vec{\mu}_i E_{ij}^{Q} Q_j = \eta \frac{R_{ij} R_{ji}}{R_{ji}^6} Q_i Q_j,$$
$$\vec{\mu}_i E_{ij}^{\mu} \vec{\mu}_j = \eta^2 \frac{R_{ij} R_{ji}}{R_{ji}^9} Q_i Q_j, \tag{19}$$

where $\vec{\mu}_i$ is the dipole moment of the nanoparticle of index i, E_{ij}^{Q} is the electrical field created by charge Q_j and acting at a moment $\vec{\mu}_i$, E_{ij}^{μ} is defined similarly, η is the NP polarizability, $\vec{\mu}_i E_{ij}^{Q} Q_j$ denotes the NP dipole–monopole interactions, and $\vec{\mu}_i E_{ij}^{\mu} \vec{\mu}_j$ denotes the NP dipole–dipole interactions. Applying these contributions to the previously calculated NP charges in Eq. (18), it is possible to calculate the effect of dipole interactions on the plasmon frequencies (see columns 3 and 8 of Table I).

CALCULATIONS OF CTPs IN SPECIFIC NP–GRAPHENE COMPLEXES

As examples of solving Eq. (18), the plasmon frequencies for several systems of nanoparticles on graphene were calculated. These were used in the following systems: (a) square of 4 NPs; (b) linear chain of 7 NPs; (c) ring of 6 NPs; and (d) a square array of 5 × 5 NPs (see Fig. 4).

In all cases, the graphene carrier density was chosen as $\rho = 5 \times 10^{12}$ cm^{-2}, which is common for the graphene under action of a gate electrode voltage, the radius of NPs was $R = 30$ nm, the interparticle distances were $h = 10R$, and the contact spot was $R_0 = 0.32R$. Due to the fact that NPs can have a contact spot with graphene of different sizes, this parameter must be selected as an external parameter of the model. Obviously, CTP frequencies will depend on this parameter. We also carried out calculations for

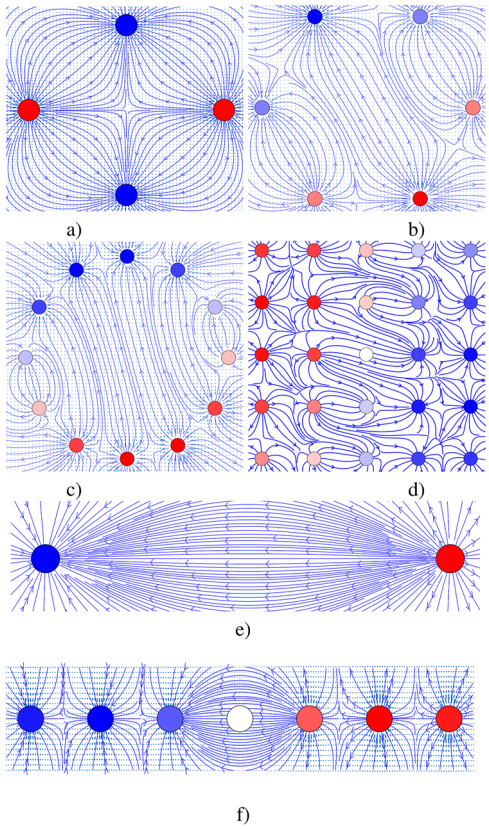

FIG. 4. Clusters of NPs with radius R = 30 nm on graphene. The distance between the nearest NPs $R_{ik} = 10 \times R$. The circle size indicates the radius of the NPs. The colors and saturation indicate the distribution of effective NP oscillating charges: Blue denotes the negative charge; red denotes the positive charge. The arrows show the electric field created by the NPs. (a) A square of NPs; (b) a hexagon of NPs; (c) a circle of NPs; (d) a 5 × 5 grid of NPs; (e) a dimer of NPs; and (f) a chain of 7 NPs.

the dimer with the above-mentioned parameters and the different values of $R_0 = 0.27R$. The calculated lowest CTP frequencies ν_i are presented in Table I. In addition, in Fig. 5, we present the dependence of the lowest CTP plasmon frequencies $\nu_{\min}$ for all these systems on density ρ of carriers in graphene. In this case, the radius of all nanoparticles R was equal to 5 nm, the interparticle distances were equal to $5R$ and $7R$, and the contact spot was $R_0 = 0.32R$. One can see that this dependence reflects the factorization in Eq. (18).

In practice, surface plasmons are often encountered, which are realized at a flat metal–dielectric interface. At the same frequency for such plasmons, the wave vector k of a surface plasmon is greater than the wave vector of a photon in free space, and therefore, the direct excitation of a surface plasmon by ordinary photons is impossible. To remedy this, various kinds of defects, gratings, etc., are used. Due to the linear law of dispersion of free photons $\omega = ck$ and the small value of the frequency in the terahertz range, it is obvious that the size L of the system, where the external

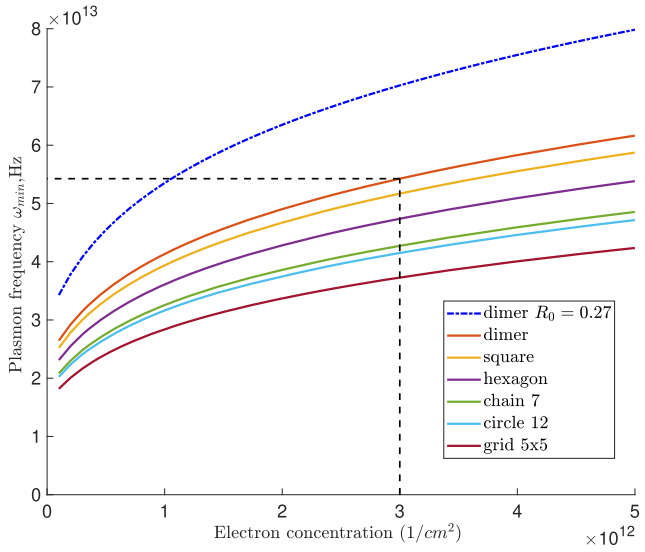

FIG. 5. Dependence of the minimum CTP frequencies $\nu_{\min}$ on the electron concentration ρ in graphene for different systems: The red line indicates the $\nu_{\min}$ dependence for the NP dimer; the yellow line is for the square of 4 NPs; the purple line is for the hexagon of 6 NPs, the green line for the chain of 7 NPs, the turquoise line is for the ring of 12 NPs, the brown line is for the grid of 5 × 5 NPs, and the blue dotted-dashed line is for the NPs dimer with parameter $R_0 = 0.27R$. The black dashed line corresponds to the parameters used in the FEM calculations (see Fig. 6).

electromagnetic field intensively interacts with the surface plasmon, will be very large $L \sim 1$–$100\ \mu$m. For the CTPs in the systems studied here, the plasmon frequencies are determined not by the wave vectors, but by the conductivity σ of the conducting surface, by the geometry of the arrangement of metal nanoparticles R_i, and by their radius R. Therefore, it can be expected that such plasmons can be easily excited by applying an external electromagnetic field of an appropriate frequency.

COMPARISON WITH THE FINITE ELEMENT METHOD

To verify our model predictions, we calculated the extinction spectrum of a dimer that comprised of two identical spherical Au NPs of radius R = 5 nm located on the graphene monolayer surface using the finite element method (FEM), realized in the COMSOL Multiphysics software. The tabulated values for n and k of Au were obtained from Ref. 43. The frequency-dependent graphene conductivity $\sigma(\omega, E_f)$ was calculated for the electron density $n = 3 \times 10^{12}/\text{cm}^2$, corresponding to $E_f = 0.2$ eV (7), $\tau = 10^{-13}$ s, and temperature $T = 300$ K. The conductivity σ was calculated by taking into account the intraband contribution $\sigma_{intra}(\omega, E_f)$ only and by taking into account both the intraband and interband $\sigma_{intra}(\omega, E_f) + \sigma_{inter}(\omega, E_f)$ contributions [see (5) and (6)]. In both cases, no significant changes were observed.

It is known that calculating an optical response of a finite size structure requires a double calculation. So, first, the field distribution in the system was calculated in the absence of particles on the infinite size graphene layer. Then, the finite size system was calculated, wherein the size of the computational domain in the direction orthogonal to the wave vector was chosen to be 150 nm, with a computational mesh containing more than 93 000 vertices.

As a result of the FEM calculations, an extinction spectrum of Au NPs dimer on the graphene surface is shown in Fig. 6. One can see that a CTP excitation emerges at $\lambda = 5320$ nm when the particles are located at the distance $h = 5R$ and at $\lambda = 5580$ nm for $h = 7R$. The CTP quality factor Q is about 7–9, which is in good agreement with our estimations discussed above. For comparison, the thick vertical dashed lines show the wavelengths calculated using our analytical model [see Eq. (18)]. It is also interesting to compare the numerical efficiency of calculations using the FEM method and using the proposed model. FEM calculations of dimer extinction spectra take more than 24 h on an AMD Ryzen Threadripper 3970x CPU with 32 cores. Calculations of the dimer CTP frequencies using our model on 1 core of a similar CPU took ~10 s.

Energy losses of CTPs in NP–graphene complexes

The energy losses of CTPs are convenient to determine by using the quality factor Q, which is the ratio of the energy losses ΔE over one oscillation period to the total energy E_{tot} of the oscillation. Here, we estimate Q using calculations of the energy losses during movement of the charge carriers both inside the nanoparticles ΔE_{NP} and inside the graphene ΔE_{Gr},

$$Q = \frac{E_{tot}}{\Delta E} = \frac{E_{tot}}{\Delta E_{NP} + \Delta E_{Gr}} \Rightarrow Q^{-1} = \frac{\Delta E_{NP}}{E_{tot}} + \frac{\Delta E_{Gr}}{E_{tot}} = Q_{NP}^{-1} + Q_{Gr}^{-1}, \quad (20)$$

where Q_{NP}^{-1} is the inverse quality factor determined by the losses in the NPs and Q_{Gr}^{-1} is the inverse quality factor determined by losses in the graphene.

Energy losses in NPs

We assume that energy losses during electron density oscillations on an individual nanoparticle are practically independent

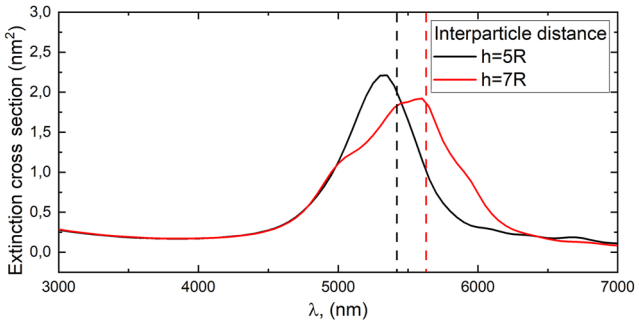

FIG. 6. FEM calculations of the extinction spectrum of Au NPs dimer on graphene at $R_0 = 0.32R$. The radius of NPs is $R = 5$ nm, the interparticle distances are $h = 5R$ (black line) and $h = 7R$ (red line). The dashed lines show the position of the CTP resonance calculated using the model.

of the density oscillations on other nanoparticles, so they can be considered independently. Energy losses during the movement of charge carriers inside a spherical NP of index i ΔE_{NP_i} can be calculated by imagining that charges move from the surface of a charged nanoparticle of radius R_i through its volume to the contact spot with graphene of radius R_0, where they transfer to graphene. In our work,[31] it is shown that the additional charges on a nanoparticle are located on its surface and that the electrical capacitance C of the nanoparticle matches well with its radius, confirming the electrostatic law for the capacitance of the sphere. Using the quasi-stationary approximation (see the arguments above), the charges inside the NP volume can be neglected. In this case, the time average energy loss in NP can be calculated as $\Delta E_{NP_i} = \langle \int_{V_i} j(r)E(r)dV \rangle = \frac{1}{\sigma_{NP}(\omega)} \int_{V_i} j^2(r)dV$, where V_i is the volume of NP of index i, j(r) is the magnitude of current inside the NP, and $\sigma_{NP}(\omega)$ is the nanoparticle optical conductivity. Because of that, this volume integral is difficult to calculate and we estimate it by replacing it with the integral over the volume of a truncated cone, of which the upper flat surface with radius $R_1 = 2R$ coincides with the NP surface. Here, the radius of the cone's lower surface is equal to the NP–graphene contact spot radius $R_0 = \eta R$ and the cone height is H (see Fig. 7).

Assuming that all NPs have the same radius R and that the volume of the cone coincides with the volume of the nanoparticle, one can get $V_{NP} = 4/3\pi R^3 \simeq V_{cone} = 1/3\pi H(R_1^2 + R_0^2 + R_1R_0)$, where $H = \frac{R}{1+\frac{\eta}{2}+\frac{\eta^2}{4}}$. Such a change in the geometry makes it easy to estimate the energy losses in NPs by Joule heating. Assuming that the current density $j(r)$ in any horizontal plane h of the cone is constant $j(r) \to j(h)$ and that the section of the cone by this plane forms a circle of radius $r(h)$, the current density in the quasi-stationary approximation can be calculated from $j(h)\pi r^2(h) = j(H)\pi R_1^2 = \dot{Z}_i$, where $\dot{Z}_i$ is the rate of change of the total charge of the NP of the index i. Using the formula for the truncated cone $r(h) = R_0 + \frac{R_1 - R_0}{H}h$, one can get

$$\Delta E_{NP_i} \simeq \frac{\dot{Z}_i^{\,2}}{\pi\sigma_{NP}(\omega)} \int_0^H \frac{dh}{r^2(h)} = \frac{\dot{Z}_i^{\,2}}{\pi\sigma_{NP}(\omega)} \frac{H}{R_0R_1} = \frac{\dot{Z}_i^{\,2}}{2\pi\sigma_{NP}(\omega)} \frac{1}{\eta R\left(1+\frac{\eta}{2}+\frac{\eta^2}{4}\right)}. \quad (21)$$

Keeping in mind that the charges of the nanoparticles are changed harmonically $Z_i = Z_i(0)e^{i\omega t}$ and the normalization of the CTP eigenvectors $\sum_i Z_i^2 = 1$, Eq. (21) is transformed into the average total energy loss in the complex of nanoparticles,

$$\Delta E_{NP} = \sum_i \Delta E_{NP_i} = \frac{-\omega^2}{2\pi\sigma_{NP}(\omega)} \frac{1}{\eta R\left(1+\frac{\eta}{2}+\frac{\eta^2}{4}\right)}. \quad (22)$$

The calculation of ΔE_{NP} requires knowledge of $\sigma_{NP}(\omega)$. For definiteness, we assume that the NPs are composed of gold. Taking into account that we use the terahertz frequency range, one can use the Drude free electron approximation[44,45] for optical conductivity since the gold interband transitions can be neglected in this frequency range. So, $\sigma_{NP}(\omega)$ can be separated into real and imaginary parts,

$$\sigma_{NP} = \frac{\sigma_0}{1-i\omega\tau} = \frac{\omega_{pl}^2\tau}{4\pi(1-i\omega\tau)} = \sigma_{NP_{Re}} + \sigma_{NP_{Im}} = \frac{\omega_{pl}^2\tau}{4\pi(1+\omega^2\tau^2)} + i\frac{\omega_{pl}^2\omega\tau^2}{4\pi(1+\omega^2\tau^2)}. \quad (23)$$

For gold, the plasma frequency $\omega_{pl} = 9.1$ eV $= 2.20 \times 10^{15}$/s,[46] while the carrier momentum relaxation time $\tau \cong 9.3 \times 10^{-15}$ s.[45,47] Since the energy loss is due to the Joule heating associated with the real part of the conductivity, we must use only the real part of the optical conductivity $\sigma_{NP}(\omega) \simeq \frac{\omega_{pl}^2\tau}{4\pi(1+\omega^2\tau^2)}$ in the ΔE_{NP} calculations. Taking into account that the total energy of oscillations in the system is equal to the maximum potential energy $E_{tot} = \sum_i \frac{Z_i^2}{2R} = \frac{1}{2R}$ and using Eqs. (22) and (23), one can get

$$Q_{NP}^{-1} = \frac{\Delta E_{NP}}{E_{tot}} = \frac{8\pi}{\eta R\left(1+\frac{\eta}{2}+\frac{\eta^2}{4}\right)} \cdot \left(\frac{\omega}{\omega_{pl}}\right)^2 \frac{(1+\omega^2\tau^2)}{\omega\tau}. \quad (24)$$

Energy losses in graphene

To calculate energy losses in graphene, it is necessary to take into account the damping factor in the intraband optical conductivity $\sigma_{intra}(\omega, E_f)$, which is determined by the scattering time τ [see Eq. (5)]. Using Eqs. (16) and (18), one can get $\omega_i\left(\omega_i + \frac{i}{\tau}\right)$

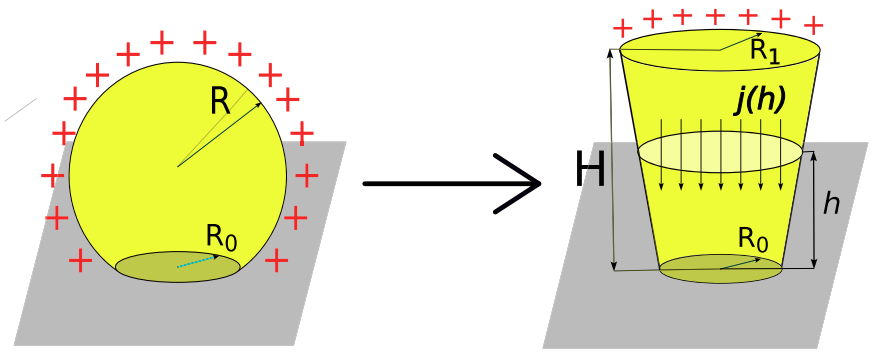

FIG. 7. Transformation of the NP geometry for energy loss calculations.

= eigenvalues$(\hat{A}^{-1}\hat{B})/\alpha$, where α is defined in Eq. (17) that has two solutions for ω_i, which differ only in the sign of the real part of the frequency,

$$\omega_i = \frac{1}{2\tau}\left(\pm\sqrt{4\tau^2 \cdot \text{eigenvalues}(\tilde{A}^{-1}\tilde{B}) - 1} - i\right). \tag{25}$$

Taking only one solution with a positive sign of the real part of the frequency, we obtain the spectrum of all oscillation frequencies that have real and imaginary parts. The imaginary part of the frequencies gives the energy loss in the graphene for oscillation mode $\Delta E_{Gr,i}$ as

$$\frac{\Delta E_{Gr,i}}{E_{Gr,i}} = \frac{\omega_{i,\text{Im}}}{\omega_{i,\text{Re}}}. \tag{26}$$

Recalling again that for harmonic vibrations, the total energy of mode i is equal to the double of the average kinetic energy of the carriers in graphene E_{Gr_i} and using the scattering time $\tau = 7 \times 10^{-14}$ s[14] for the specific case of a CTP in the dimer consisting of two nanoparticles of radius $R = 5$ nm located on graphene at a distance $L = 7R$ from each other, one can obtain the value $\frac{\Delta E_{Gr_i}}{1/2E_{tot}} = 2Q_{Gr}^{-1} = \frac{\omega_{i,\text{Im}}}{\omega_{i,\text{Re}}} \simeq 0.02$. Therefore, taking Eq. (20) into account, one can estimate the quality factor of the graphene subsystem as $Q \sim 50$.

Using Eqs. (24) and (26), we have calculated the dependence of the CTP quality factor on the radius R for two gold nanoparticles at a distance of $L = 7R$, where the carrier concentration is equal to $n_e = 10^{12}$/cm (see Fig. 8).

INTERACTION OF CTPs WITH EXTERNAL ELECTROMAGNETIC FIELDS

In order to understand how the considered CTPs can be excited, it is necessary to calculate the interaction constant of the plasmons and the external electromagnetic field (EMF). For simplicity, we assume that the external EMF is incident on graphene normally. Due to the nanometer size of the system and the EMF wavelength being in the THz range $\lambda \gg 10$ μm, we assume that the external EMF does not depend on the coordinates $\vec{E}_{ext}(r,\omega) = E^0_{ext}\vec{P}_{ext}$. By analogy with Eq. (4), it is possible to write down the power of the absorption of the external electromagnetic field W_{ext} energy as

$$W_{ext} = \frac{1}{2}\int_\Omega \vec{j}(r,\omega)\vec{E}^*_{ext}(r,\omega)\, d^2r = \frac{1}{2}\sigma(\omega)E^0_{ext}\int_\Omega \vec{E}(r)\vec{P}_{ext}\, d^2r$$
$$= \frac{1}{2}\sigma(\omega)E^0_{ext}\int_\Omega \vec{\nabla}(\varphi(r)\vec{P}_{ext})\, d^2r. \tag{27}$$

Using (9) and (12) and the Taylor series expansion: $\frac{1}{|r-R_j|} = \frac{1}{|R_j|}\left[1 + \frac{\vec{r}\vec{n}_j}{|R_j|}\right]$, where $\vec{n}_j = \frac{\vec{R}_j}{|R_j|}$, Eq. (27) is transformed as

$$W_{ext} = \frac{1}{2}\sigma(\omega)E^0_{ext}\sum_{j,k}\frac{Q_j}{|R_j|}\int_0^{2\pi}\left[1 + \frac{\vec{r}\vec{R}_j}{|R_j|}\right)\vec{n}(r - R_k)\vec{P}_{ext}d\phi.$$

Shifting the origin to the point $\vec{R}_k$, replacing $\sigma(\omega)$ by $\sigma_{intra}(\omega, E_f)$ and remembering that the radius vector $r = R_0$ when integrating along the circular contour C, this equation is transformed as

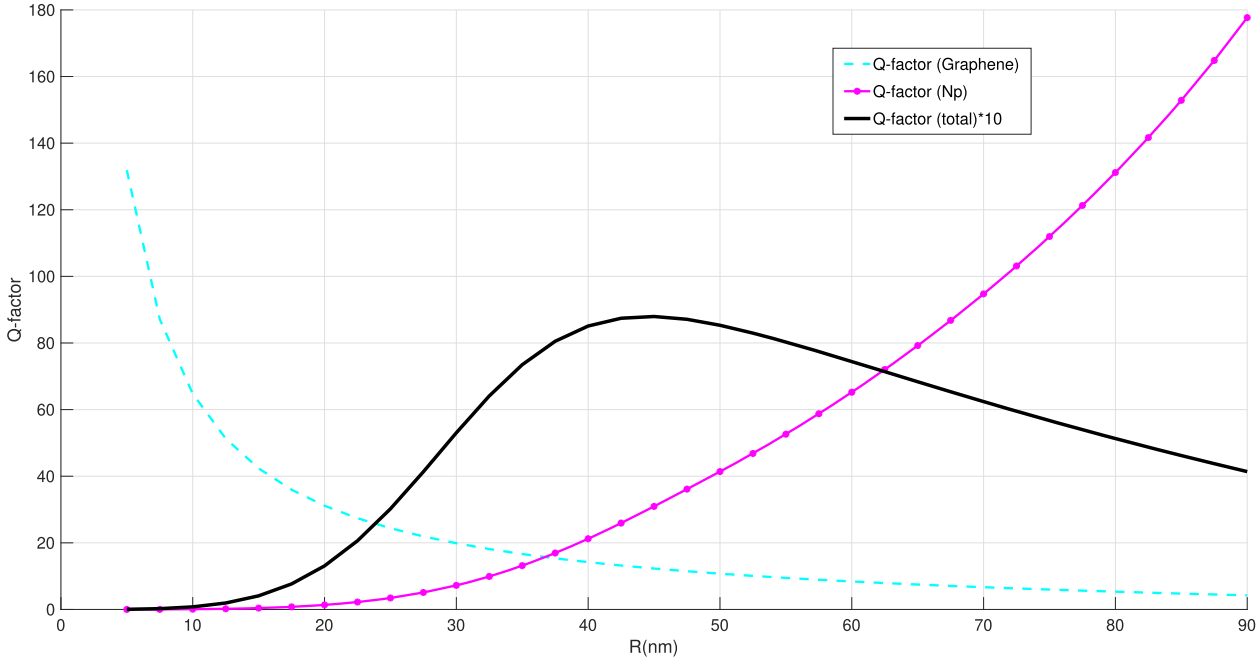

FIG. 8. Dependence of the dimer quality factor and its contributions on the radius R of NPs.

$$W_{ext} = \frac{1}{2}\sigma(\omega)E^0_{ext}\sum_{j,k}\frac{Q_j}{|R_j|^2}\int_0^{2\pi}(\vec{r}\vec{n}_{jk})(\vec{n}_r\vec{P}_{ext})d\phi$$
$$\simeq \frac{\pi}{2}\sigma_{intra}(\omega, E_f)E^0_{ext}\sum_{j,k}\frac{Q_jR_0}{|R_{jk}|^2}\cos(\vec{R}_{jk}, \vec{P}_{ext}). \quad (28)$$

The normalized interaction constants W_{ext} for some systems are presented in Table I.

Additionally, we decide to test the hypothesis that W_{ext} is proportional to the scalar product of the dipole moment $\vec{d}$ of the oscillating charges Q_j of the NPs on graphene and the EMF electric field polarization vector $\vec{P}_{ext}$,

$$W_{ext} = \vec{P}_{ext}\sum_j Q_j\vec{R}_j = \vec{d}\vec{P}_{ext}. \quad (29)$$

In other words, we assume that the EMF absorption power is spent on the formation of the charges Q_j located at points with coordinates $\vec{R}_i$. The columns 4, 5, 9, and 10 of Table I present the normalized absorption power coefficients W_{ext}, calculated by (28) (top lines) and by (29) (bottom lines). Notably, these coefficients calculated by both the formulas match well in most cases, which suggests the possibility of using the simplified formula in (29) to estimate the interaction constant of an EMF with plasmonic modes. It can also be noticed that some plasmonic modes do not interact with the external electromagnetic field, something that can be explained by their spatial symmetry [see also Fig. 4(a)].

DISCUSSION

In recent years, charge transfer plasmons (CTPs) have been investigated in systems consisting of two or more metal NPs, connected by a conductive junction (bridge). In such systems, free charges flow between the nanoparticles, leading to the appearance of CTP oscillations, of which the frequency usually resides in the Vis–IR frequency region,[31,48–51] with the CTPs being accompanied by an oscillating electric current through the nanoparticle junctions. Depending on the type of nanostructures and bridges, this charge transfer can be analyzed through quantum tunneling and by classical conducting bridge calculations.[52–55] It should be noted that the quantum tunneling effect is important for very small distances between nanoparticles (<5 Å) only (see, for example, Ref. 55). It is shown that the intensity, spectral width, and resonance frequency of the CTPs depend directly on the conductance of the junction,[31,49,56–59] wherein the CTPs can be used to create terahertz-frequency photonic devices[60] and ultrafast nanoswitches.[61]

The purpose of this work was to develop a theory and theoretically study CTPs in systems where the charge oscillates between metal NPs, not utilizing conductive bridges, but a graphene surface to connect them. The applied model takes into account the kinetic energy of the carriers inside the graphene as well as the Coulomb energy of the charged nanoparticles and includes energy dissipation.

The properties of the CTPs were investigated for NP complexes on a single-layer graphene surface using the assumption that the charge density in the doped graphene is much greater than the charge density induced during the CTP oscillations. Linear equations were obtained that describe the CTP frequencies and their eigenvectors, i.e., amplitudes of oscillating charges for each NP. It was shown that the plasmon frequencies reside in the THz range and that they can be factorized, i.e., they can be presented as a product of a factor determined by the graphene Fermi level and a factor determined by the complex geometry of the NPs, wherein the monopole–dipole and dipole–dipole interactions are taken into account. CTP frequencies and eigenvectors were calculated for several different geometries of NP–graphene complexes, namely for a dimer, a square of 4 NPs, rings of 6 and 12 NPs, and a square array of 5 × 5 NPs. It was shown for all these systems with the same NP size and interparticle distances that the CTP frequencies differ by less than a factor of two.

To demonstrate the numerical efficiency of the model, the CTP frequency of the dimer was also calculated using the finite element method (FEM) and a good agreement for the calculated CTP frequencies by the two methods could be demonstrated. Importantly, the speed of calculations according to the proposed model is approximately 3–4 orders higher than the speed when using the FEM method, so the model makes it possible to calculate CTPs for very large systems.

The dissipation of the CTP energy and, correspondingly, the quality factors (Q) have also been addressed. The Q factors, with predicted values of ~10 − 100, are determined by two competing partial factors: the carrier energy losses inside the NPs and in the graphene. It was found that the energy losses in the NPs are inversely dependent on the radius of the nanoparticles, while the losses in graphene are proportional to the NP radius and the distance between them.

For the investigated NP–graphene systems, the magnitude of oscillating NP charges Q_i and the electric field distributions were analyzed for various CTP modes, showing that different plasmon modes interact differently with an applied exciting EMF. The interaction constants (absorption power W_{ext}) of the CTPs with an exciting EMF were calculated, showing that W_{ext} is proportional to the product of the CTP dipole moment and the polarization vector $\vec{P}_{ext}$ of the EMF.

The proposed quantum–classical model may be useful to calculate CTP properties in the THz range for large NP–graphene systems with a considerable degree of accuracy. This possibility can be very useful for the prediction of properties of different THz devices, especially in the fields of drug and explosive detection, biosensors used in medical sciences, security screening, and photonic devices. We also believe that the proposed NP–graphene systems constitute a highly relevant perspective for the modern, swiftly developing, THz technology, such as the new generation mobile communication technology, due to the fact that the use of NPs of 30–100 nm size will lead to miniaturization of the elements that cannot be achieved using plasmons in pure graphene or graphene nanoribbons.

ACKNOWLEDGMENTS

This study was funded by the Ministry of Science and High Education of Russian Federation, Project No. FSRZ-2023-0006. The calculations of CTPs in specific NP–graphene complexes were performed within the RSF Grant No. 23-12-20007 and the Krasnoyarsk Territorial Foundation for Support of Scientific and R & D Activities, Agreement No. 256. H. Ågren was supported by the Swedish Science Research Council on Contract No. 2022-03405.

AUTHOR DECLARATIONS

Conflict of Interest

The authors have no conflicts to disclose.

Author Contributions

A. S. Fedorov: Conceptualization (equal); Formal analysis (equal); Funding acquisition (equal); Investigation (equal); Methodology (equal); Project administration (equal); Supervision (equal); Validation (equal); Writing – original draft (equal); Writing – review & editing (equal). **E. V. Eremkin**: Conceptualization (equal); Formal analysis (equal); Investigation (equal); Methodology (equal); Software (equal); Supervision (equal); Visualization (equal); Writing – original draft (equal). **P. O. Krasnov**: Formal analysis (equal); Investigation (equal); Methodology (equal); Software (equal); Visualization (equal); Writing – original draft (equal). **V. S. Gerasimov**: Formal analysis (equal); Investigation (equal); Methodology (equal); Software (equal); Writing – original draft (equal). **H. Ågren**: Conceptualization (equal); Formal analysis (equal); Investigation (equal); Software (equal); Writing – original draft (equal); Writing – review & editing (equal). **S. P. Polyutov**: Conceptualization (equal); Formal analysis (equal); Funding acquisition (equal); Investigation (equal); Methodology (equal); Project administration (equal); Supervision (equal); Validation (equal); Writing – review & editing (equal).

DATA AVAILABILITY

The data that support the findings of this study are available within the article.

REFERENCES

[1] M. Tonouchi, "Cutting-edge terahertz technology," Nat. Photonics **1**, 97–105 (2007).
[2] P. Jepsen, D. Cooke, and M. Koch, "Terahertz spectroscopy and imaging—Modern techniques and applications," Laser Photonics Rev. **5**, 124–166 (2010).
[3] X. Yang, X. Zhao, K. Yang, Y. Liu, Y. Liu, W. Fu, and Y. Luo, "Biomedical applications of terahertz spectroscopy and imaging," Trends Biotechnol. **34**, 810–824 (2016).
[4] Y.-S. Lee, *Principles of Terahertz Science and Technology* (Springer, Boston, MA, 2009).
[5] M. Lee and M. C. Wanke, "Searching for a solid-state terahertz technology," Science **316**, 64–65 (2007).
[6] B. S. Williams, "Terahertz quantum-cascade lasers," Nat. Photonics **1**, 517–525 (2007).
[7] R. Paiella, *Comprehensive Semiconductor Science and Technology*, edited by P. Bhattacharya, R. Fornari, and H. Kamimura (Elsevier, Amsterdam, 2011), pp. 683–723.
[8] N. M. Burford and M. O. El-Shenawee, "Review of terahertz photoconductive antenna technology," Opt. Eng. **56**, 010901 (2017).
[9] F. H. L. Koppens, D. E. Chang, and F. J. García de Abajo, "Graphene plasmonics: A platform for strong light–matter interactions," Nano Lett. **11**, 3370–3377 (2011).
[10] P. Tassin, T. Koschny, and C. M. Soukoulis, "Graphene for terahertz applications," Science **341**, 620–621 (2013).
[11] T. Low and P. Avouris, "Graphene plasmonics for terahertz to mid-infrared applications," ACS Nano **8**, 1086–1101 (2014).
[12] A. Tredicucci and M. S. Vitiello, "Device concepts for graphene-based terahertz photonics," IEEE J. Sel. Top. Quantum Electron. **20**, 130–138 (2014).
[13] J. König-Otto, M. Mittendorff, T. Winzer, F. Kadi, E. Malic, A. Knorr, C. Berger, W. de Heer, A. Pashkin, H. Schneider, M. Helm, and S. Winnerl, "Slow noncollinear Coulomb scattering in the vicinity of the Dirac point in graphene," Phys. Rev. Lett. **117**, 087401 (2016).
[14] K. Bolotin, K. Sikes, Z. Jiang, M. Klima, G. Fudenberg, J. Hone, P. Kim, and H. Stormer, "Ultrahigh electron mobility in suspended graphene," Solid State Commun. **146**, 351–355 (2008).
[15] X. Du, I. Skachko, A. Barker, and E. Y. Andrei, "Approaching ballistic transport in suspended graphene," Nat. Nanotechnol. **3**, 491–495 (2008).
[16] A. S. Mayorov, R. V. Gorbachev, S. V. Morozov, L. Britnell, R. Jalil, L. A. Ponomarenko, P. Blake, K. S. Novoselov, K. Watanabe, T. Taniguchi, and A. K. Geim, "Micrometer-scale ballistic transport in encapsulated graphene at room temperature," Nano Lett. **11**, 2396–2399 (2011).
[17] V. Ryzhii, M. Ryzhii, V. Mitin, and M. S. Shur, "Graphene tunneling transit-time terahertz oscillator based on electrically induced p–i–n junction," Appl. Phys. Express **2**, 034503 (2009).
[18] J. H. Gosling, O. Makarovsky, F. Wang, N. D. Cottam, M. T. Greenaway, A. Patanè, R. D. Wildman, C. J. Tuck, L. Turyanska, and T. M. Fromhold, "Universal mobility characteristics of graphene originating from charge scattering by ionised impurities," Commun. Phys. **4**, 1–8 (2021).
[19] Q. Guo, C. Li, B. Deng, S. Yuan, F. Guinea, and F. Xia, "Infrared nanophotonics based on graphene plasmonics," ACS Photonics **4**, 2989–2999 (2017).
[20] S. Xiao, X. Zhu, B.-H. Li, and N. A. Mortensen, "Graphene-plasmon polaritons: From fundamental properties to potential applications," Front. Phys. **11**, 117801 (2016).
[21] A. Vakil and N. Engheta, "Transformation optics using graphene," Science **332**, 1291–1294 (2011).
[22] N. M. R. Peres, "Colloquium: The transport properties of graphene: An introduction," Rev. Mod. Phys. **82**, 2673–2700 (2010).
[23] K. Tantiwanichapan, X. Wang, H. Durmaz, Y. Li, A. K. Swan, and R. Paiella, "Graphene terahertz plasmons: A combined transmission spectroscopy and Raman microscopy study," ACS Photonics **4**, 2011–2017 (2017).
[24] A. Pecchia, G. Penazzi, L. Salvucci, and A. Di Carlo, "Non-equilibrium Green's functions in density functional tight binding: Method and applications," New J. Phys. **10**, 065022 (2008).
[25] B. Hourahine *et al.*, "DFTB+, a software package for efficient approximate density functional theory based atomistic simulations," J. Chem. Phys. **152**, 124101 (2020).
[26] M. Elstner, D. Porezag, G. Jungnickel, J. Elsner, M. Haugk, T. Frauenheim, S. Suhai, and G. Seifert, "Self-consistent-charge density-functional tight-binding method for simulations of complex materials properties," Phys. Rev. B **58**, 7260–7268 (1998).
[27] A. Fihey, C. Hettich, J. Touzeau, F. Maurel, A. Perrier, C. Köhler, B. Aradi, and T. Frauenheim, "SCC-DFTB parameters for simulating hybrid gold-thiolates compounds," J. Comput. Chem. **36**, 2075–2087 (2015).
[28] S. Grimme, J. Antony, S. Ehrlich, and H. Krieg, "A consistent and accurate *ab initio* parametrization of density functional dispersion correction (DFT-D) for the 94 elements H-Pu," J. Chem. Phys. **132**, 154104 (2010).
[29] S. Grimme, S. Ehrlich, and L. Goerigk, "Effect of the damping function in dispersion corrected density functional theory," J. Comput. Chem. **32**, 1456–1465 (2011).
[30] S. Datta, *Electronic Transport in Mesoscopic Systems* (Cambridge University Press, 1995).
[31] A. S. Fedorov, P. O. Krasnov, M. A. Visotin, F. N. Tomilin, S. P. Polyutov, and H. Ågren, "Charge-transfer plasmons with narrow conductive molecular bridges: A quantum-classical theory," J. Chem. Phys. **151**, 244125 (2019).
[32] A. S. Fedorov, P. O. Krasnov, M. A. Visotin, F. N. Tomilin, and S. P. Polyutov, "Thermoelectric and plasmonic properties of metal nanoparticles linked by conductive molecular bridges," Phys. Status Solidi B **257**, 257 (2020).
[33] A. H. Castro Neto, F. Guinea, N. M. R. Peres, K. S. Novoselov, and A. K. Geim, "The electronic properties of graphene," Rev. Mod. Phys. **81**, 109–162 (2009).
[34] S. Das Sarma, S. Adam, E. H. Hwang, and E. Rossi, "Electronic transport in two-dimensional graphene," Rev. Mod. Phys. **83**, 407–470 (2011).
[35] M. Bonmann, A. Vorobiev, M. A. Andersson, and J. Stake, "Charge carrier velocity in graphene field-effect transistors," Appl. Phys. Lett. **111**, 233505 (2017).

[36]L. D. Landau, E. M. Lifshitz, L. P. Pitaevskii *et al.*, *Electrodynamics of Continuous Media*, *Course of Theoretical Physics*, 2nd ed. (Butterworth-Heinemann, Oxford, England, 1984).
[37]V. P. Gusynin, S. G. Sharapov, and J. P. Carbotte, "Sum rules for the optical and Hall conductivity in graphene," Phys. Rev. B **75**, 165407 (2007).
[38]X. Luo, T. Qiu, W. Lu, and Z. Ni, "Plasmons in graphene: Recent progress and applications," Mater. Sci. Eng.: R: Rep. **74**, 351–376 (2013).
[39]L. A. Falkovsky and A. A. Varlamov, "Space-time dispersion of graphene conductivity," Eur. Phys. J. B **56**, 281–284 (2007).
[40]J. M. Dawlaty, S. Shivaraman, J. Strait, P. George, M. Chandrashekhar, F. Rana, M. G. Spencer, D. Veksler, and Y. Chen, "Measurement of the optical absorption spectra of epitaxial graphene from terahertz to visible," Appl. Phys. Lett. **93**, 131905 (2008).
[41]V. J. Katz, "The history of Stokes' theorem," Math. Mag. **52**, 146–156 (1979).
[42]A. S. Fedorov, M. A. Visotin, E. V. Eremkin, P. O. Krasnov, H. Ågren, and S. P. Polyutov, "Charge-transfer plasmons of complex nanoparticle arrays connected by conductive molecular bridges," Phys. Chem. Chem. Phys. **24**, 19531–19540 (2022).
[43]M. A. Ordal, R. J. Bell, R. W. Alexander, L. L. Long, and M. R. Querry, "Optical properties of Au, Ni, and Pb at submillimeter wavelengths," Appl. Opt. **26**, 744 (1987).
[44]P. Drude, "Zur Elektronentheorie der Metalle," Ann. Phys. **306**, 566–613 (1900).
[45]S. Maier, *Plasmonics: Fundamentals and Applications* (Springer, New York, 2007).
[46]F. Kopitzki, *Zur Quantenmechanik laserbestrahlter Festkörper* (Physikalisches Institut; Physikalisches Inst., Bonn IR, 1993).
[47]P. B. Johnson and R. W. Christy, "Optical constants of the noble metals," Phys. Rev. B **6**, 4370–4379 (1972).
[48]F. Wen, Y. Zhang, S. Gottheim, N. S. King, Y. Zhang, P. Nordlander, and N. J. Halas, "Charge transfer plasmons: Optical frequency conductances and tunable infrared resonances," ACS Nano **9**, 6428–6435 (2015).
[49]A. N. Koya and J. Lin, "Charge transfer plasmons: Recent theoretical and experimental developments," Appl. Phys. Rev. **4**, 021104 (2017).
[50]W. Zhu, R. Esteban, A. G. Borisov, J. J. Baumberg, P. Nordlander, H. J. Lezec, J. Aizpurua, and K. B. Crozier, "Quantum mechanical effects in plasmonic structures with subnanometre gaps," Nat. Commun. **7**, 11495 (2016).
[51]A. Fedorov, M. Visotin, V. Gerasimov, S. Polyutov, and P. Avramov, "Charge transfer plasmons in the arrays of nanoparticles connected by conductive linkers," J. Chem. Phys. **154**, 084123 (2021).
[52]K. J. Savage, M. M. Hawkeye, R. Esteban, A. G. Borisov, J. Aizpurua, and J. J. Baumberg, "Revealing the quantum regime in tunnelling plasmonics," Nature **491**, 574–577 (2012).
[53]J. A. Scholl, A. García-Etxarri, A. L. Koh, and J. A. Dionne, "Observation of quantum tunneling between two plasmonic nanoparticles," Nano Lett. **13**, 564–569 (2013).
[54]A. Wiener, H. Duan, M. Bosman, A. P. Horsfield, J. B. Pendry, J. K. W. Yang, S. A. Maier, and A. I. Fernández-Domínguez, "Electron-energy loss study of nonlocal effects in connected plasmonic nanoprisms," ACS Nano **7**, 6287–6296 (2013).
[55]R. Esteban, A. G. Borisov, P. Nordlander, and J. Aizpurua, "Bridging quantum and classical plasmonics with a quantum-corrected model," Nat. Commun. **3**, 825 (2012).
[56]O. Pérez-González, N. Zabala, A. G. Borisov, N. J. Halas, P. Nordlander, and J. Aizpurua, "Optical spectroscopy of conductive junctions in plasmonic cavities," Nano Lett. **10**, 3090–3095 (2010).
[57]I. Romero, J. Aizpurua, G. W. Bryant, and F. J. García De Abajo, "Plasmons in nearly touching metallic nanoparticles: Singular response in the limit of touching dimers," Opt. Express **14**, 9988–9999 (2006).
[58]J. Fontana and B. R. Ratna, "Highly tunable gold nanorod dimer resonances mediated through conductive junctions," Appl. Phys. Lett. **105**, 011107 (2014).
[59]A. N. Koya and J. Lin, "Bonding and charge transfer plasmons of conductively bridged nanoparticles: The effects of junction conductance and nanoparticle morphology," J. Appl. Phys. **120**, 093105 (2016).
[60]J. Gu, R. Singh, X. Liu, X. Zhang, Y. Ma, S. Zhang, S. A. Maier, Z. Tian, A. K. Azad, H.-T. Chen, A. J. Taylor, J. Han, and W. Zhang, "Active control of electromagnetically induced transparency analogue in terahertz metamaterials," Nat. Commun. **3**, 1151 (2012).
[61]N. Large, M. Abb, J. Aizpurua, and O. L. Muskens, "Photoconductively loaded plasmonic nanoantenna as building block for ultracompact optical switches," Nano Lett. **10**, 1741–1746 (2010).